Soft Matter

Accepted Manuscript

This article can be cited before page numbers have been issued, to do this please use: T. Athanasiou, B. Mei, K. S. Schweizer and G. Petekidis, *Soft Matter*, 2025, DOI: 10.1039/D4SM01428F.

ROYAL SOCIETY OF CHEMISTRY

rsc.li/soft-matter-journal

View Article Online
DOI: 10.1039/D4SM01428F

Probing cage dynamics in concentrated hard-sphere suspensions and glasses with high frequency rheometry

THANASIS ATHANASIOU [1,2], BAICHENG MEI [*3], KENNETH S. SCHWEIZER [*3,4]

AND GEORGE PETEKIDIS [*1,2]

[1]*Institute of Electronic Structure & Laser, FORTH, Heraklion, 70013 Greece*

[2]*Department of Materials Science and Technology, University of Crete, Heraklion, 70013 Greece*

[3]*Department of Material Science and Materials Research Laboratory, University of Illinois at Urbana-Champaign, Urbana, Illinois 61801, USA*

[4]*Department of Chemistry and Department of Chemical & Biomolecular Engineering, University of Illinois at Urbana-Champaign, Urbana, Illinois 61801, USA*

*georgp@iesl.forth.gr, *kschweiz@illinois.edu, *bcmei@illinois.edu

The cage concept, a central microscopic mechanism for glassy dynamics, has been utilized in concentrated colloidal suspensions to describe a number of phenomena. Here we probe the evolution of cage formation and shear elasticity with increasing volume fraction in hard sphere suspensions, with emphasis on the short-time dynamics. To this end we utilize linear viscoelastic (LVE) measurements, by means of conventional rotational rheometers and a home-made HF piezo-rheometer, to probe the dynamic response over a broad range of volume fractions up to the very dense glassy regime in proximity to random close packing. We focus on the LVE spectra and times shorter than those corresponding to the dynamic shear modulus G′ plateau, where the system is approaching transient localization and cage confinement. On these short times (higher frequencies) the dynamic cage is not yet fully developed and particles are not (strictly) transiently localized. This corresponds to an effective solid-to-liquid transition in the LVE spectrum (dynamic moduli) marked by a High Frequency (HF) crossover. On the other hand, as volume fraction increases caging becomes tighter, particles become more localized, and the onset of localization timescale becomes shorter. This onset of transient localization to shorter times shifts the HF crossover to higher values. Therefore, the study of the dependence of the HF crossover properties (frequency and moduli) on volume fraction provides direct insights concerning the onset of particle in-cage motion, and allows direct comparison with current theoretical models. We compare the experimental data with predictions of a microscopic statistical mechanical theory where qualitative and quantitative agreements are found. Findings include the discovery of microscopic mechanisms for the crossover between the two exponential dependences of the localization onset time scale and the elastic shear modulus at high volume fraction as a consequence of emergent many body structural correlations and their consequences on

View Article Online
DOI: 10.1039/D4SM01428F

dynamic constraints. Moreover, an analytic derivation of the relationship between the high frequency localized short-time scale and elastic shear modulus is provided which offers new physical insight and explains why these two variables are experimentally observed to exhibit nearly-identical behaviors.

Keywords: hard spheres, colloidal glass, caging, short time dynamics, shear elastic modulus, rheology, nonlinear Langevin equation theory, particle localization

View Article Online
DOI: 10.1039/D4SM01428F

Chapter 3 1. Introduction

Brownian hard sphere colloidal suspensions is one of the simplest model soft matter systems with its structure and dynamics extensively studied (1–3). Nevertheless, although simple in terms of constituents and their interactions, this system still poses challenges (4,5) as it exhibits rich structural, thermodynamic and mechanical behavior especially upon increasing the volume fraction towards its maximum value, or random close packing (RCP) state. In the concentrated regime, where particle surfaces approach to distances far less than their radii on average, many body interactions dominate affecting microstructure, quiescent dynamics, and viscoelasticity. These many body correlations impose significant theoretical challenges. The nature of the glass transition is still a debated topic with advances being made by comparing the physics of colloidal suspensions with molecular glass formers (6–10). While in theory, hard core interactions are defined by an infinite repulsion at contact and zero at larger distances, in a real system such as the sterically stabilized Poly-methylmethacrylate (PMMA) spheres (11) the repulsion pair potential cannot be infinitely steep (12) and the softness induced by the steric layer may affect the viscoelastic response at higher frequencies (13).

In the colloidal regime, time scales are set by the elementary Brownian time τ_0 ($= R^2/6D_0$), with R the particle radius, $D_0 = k_BT/6\pi\eta_sR$ the Stokes-Einstein-Sutherland self-diffusion coefficient at infinite dilution, k_B the Boltzmann constant, T the absolute temperature, and η_s the solvent viscosity. As the particle volume fraction increases from the dilute limit, particles start to interact via solvent-mediated hydrodynamic and excluded volume (entropic) interactions and hence the microscopic particle dynamics slow down. Eventually at volume fractions around $\phi \approx 0.4$ (14) the dynamics split into two distinct relaxation modes, one on a short length and hence short time scale (often referred to as β-relaxation in the Mode-Coupling Theory (MCT) framework) within the first neighbor distances, and one on larger and hence longer time scale, the so-called α-relaxation, where particles diffuse beyond their first neighbor shell (15,16). At the onset of the thermodynamically metastable (17) regime at $\phi \approx 0.49$, the two relaxation processes start to strongly separate in time (5). At the phenomenologically deduced glass transition volume fraction, typically cited to occur at $\phi \approx 0.58$ and determined based on the (arbitrary) practical longest time scale of a measurement or extrapolated fits of an "ideal" MCT critical power law, the inverse long-time diffusion constant and related zero-shear viscosity exhibit a sharp increase. Taking the cage model as a reference (15) the two relaxation modes have different origin: the β-

View Article Online
DOI: 10.1039/D4SM01428F

relaxation is linked to in-cage rattling (18,19) and the structural α-relaxation to thermally activated hopping or cage escape. This mobility reduction is also reflected in the mean squared displacement (MSD), $\langle \Delta r^2(t) \rangle = \langle |r(t)-r(0)|^2 \rangle$ where r(t) denotes particle position at time t and the bracket represents an ensemble average over all particle trajectories under consideration. At higher volume fractions ($\phi > 0.58$) and intermediate time scales (between α and β-relaxation) single particle motion becomes even more strongly coupled to the structure and dynamics of neighboring particles, and its subdiffusive character on intermediate time and length scales becomes more prominent. This is the regime where the localization plateau emerges, thereby separating the dynamics into long-time and short-time regimes with their diffusion coefficients D_L and D_S (20–23) corresponding to the α-relaxation and β-relaxation, respectively. Interestingly, the term β-relaxation was originally used in molecular glass formers to describe the relaxation modes that are extrinsic to the nature of glass transition (24). Note that the β-relaxation can refer to different microscopic dynamical processes in thermal molecular glasses and hard sphere colloidal glasses, although in both cases they reflect the more short-time and local motions in each system, however at different values of absolute length- and time-scales. In the colloidal field - hence in this work - it refers to the particle in-cage motion.

A similar behavior is exhibited in linear viscoelastic (LVE) spectra where dynamic moduli at low- and high-frequencies (long- and short-times respectively) are separated by the caging plateau which thereby defines the intermediate time dynamically relaxed elastic shear modulus G′, as has been shown in previous studies (25–27). When the probing frequency is decreased sufficiently (at frequencies often inaccessible to commercial rheometers) the suspension exhibits a liquid-like behavior marked by the Low-Frequency (LF) G′- G′′ crossover with a time scale $1/\omega_{c\text{-}LF}$. Similar phenomenology, but for a completely different reason, is exhibited at elevated frequencies. For these short-time observations the system appears as liquid-like as LVE probes the in-cage particle diffusion. This is reflected in the rheological response which exhibits a second solid-to-liquid transition and a relevant High Frequency (HF) G′ - G′′ crossover, at a frequency $\omega_{c\text{-}HF} > 1/\tau_0 >> \omega_{c\text{-}LF}$.

A significant amount of work in the literature has focused on the long-time α-relaxation process and the caging plateau which is the manifestation of the kinetic glass transition and the transiently localized state, respectively. The α-relaxation has been the epicenter of a debate concerning whether the literally frozen dynamics predicted by MCT (28) is true or whether the

View Article Online
DOI: 10.1039/D4SM01428F

cage has a finite lifetime due to the presence of ergodicity-restoring thermally activated hopping processes (5) as predicted by other theories (29). The latter is generally acknowledged to be the case based on dynamic scattering experiments (30,31) and direct trajectory observations (32,33). To the best of our knowledge, no systematic study has quantitatively linked the rheological signature of colloidal glasses at high frequencies with the theoretical description of short-time relaxation. Hence, its connection with elastic shear modulus remains elusive.

In this work we focus on microscopic times, and in particular a measure of the timescale for the onset of transient localization, τ_{loc}, and its relation to $1/\omega_{c\text{-}HF}$ obtained from macroscopic rheology. For the case of monodisperse spheres the LF crossover can be modeled by a single element Maxwell fluid where the relevant time scale is defined by the moduli crossover frequency. This Maxwell relaxation is linked to the long-time diffusion coefficient (34). However, this is not the case for the HF crossover where its prediction is more challenging (35). The HF crossover clearly sets a time scale, $\tau_{c\text{-}HF} = 1/\omega_{c\text{-}HF}$, and a corresponding modulus $G_{c\text{-}HF} = G'(\omega_{c\text{-}HF}) = G''(\omega_{c\text{-}HF})$ that marks the practical solid to liquid crossover transition, and should reflect the characteristic dynamics within a cage length-scale. We explore the behavior of the HF crossover by performing intermediate and high frequency small amplitude oscillatory shear experiments in a HS colloidal suspension where the volume fraction is systematically increased.

There are many direct (36) and indirect (37,38) methods to obtain high frequency LVE data, with their own merits and limitations. High frequency oscillatory shear is not possible with most commercial rheometers which are limited to frequencies up to around 200 rad/s. We utilize high frequency rheometry by means of an in-house developed piezo rheometer (PZR) capable of extending the accessible frequency range up to 7000 rad/s thus probing faster dynamics (39). The volume fraction dependence of $G_{c\text{-}HF}$ and $\omega_{c\text{-}HF}$ extracted from the LVE spectra are compared with the predictions of the Nonlinear Langevin Equation (NLE) theory within the dynamic free energy framework (40,41) and the physical mechanisms underlying our $G_{c\text{-}HF}$ and $\omega_{c\text{-}HF}$ measurements are elucidated. The relation of LVE and dynamics is briefly described in section 2 where the relevant time scales are defined. Section 3 presents the background on NLE theory followed by a materials and methods description in section 4. Theoretical predictions of NLE theory and experimental rheological data are compared and discussed in section 5, before concluding in the last section 6.

View Article Online
DOI: 10.1039/D4SM01428F

2. High frequency LVE and in-cage dynamics

The classic Stokes-Einstein-Sutherland (SE) equation relates the solvent viscosity to the single particle self-diffusion constant in the dilute limit (21). By generalizing this equation, Mason et al. related the MSD to the frequency-dependent complex modulus $G^*(\omega)$ given by (27,42):

$$G^*(\omega)=\frac{k_BT}{\pi Ri\omega\langle\Delta\hat{r}^2(t)\rangle} \quad (1)$$

where i is the imaginary unit and $\langle\Delta\hat{r}^2(t)\rangle$ the Fourier transform of the MSD. Hence,

$$G'(\omega)=|G^*(\omega)|cos\left(\frac{\pi\alpha(\omega)}{2}\right) \quad (2)$$

$$G''(\omega)=|G^*(\omega)|sin\left(\frac{\pi\alpha(\omega)}{2}\right) \quad (3)$$

where α is:

$$\alpha(\omega)=\frac{dln\langle\Delta r^2(t)\rangle}{dlnt} \quad (4)$$

Eq. (1) is one of the so-called Generalized Stokes Einstein (GSE) equations, that contrary to the simple SE equation for simple liquids, is an approximate extension to all frequencies for viscoelastic systems (27,43). Moreover, the SE equation and its generalizations do assume the validity of fluctuation dissipation theorem which in turn implies a system at thermodynamic equilibrium. Nevertheless, this is a reasonable approximation also for glassy systems where the evolution towards equilibrium is slow or completely halted, i.e. the system is at a long-lived local minimum of the free energy. This has been evidenced by microrheological experiments (44) and verified theoretically for colloidal glasses (34). In a reverse procedure, Fig. 1 demonstrates the use of linear viscoelastic data measured by a dynamic frequency sweep in the linear regime to calculate the MSD in a hard sphere glass sample.

View Article Online
DOI: 10.1039/D4SM01428F

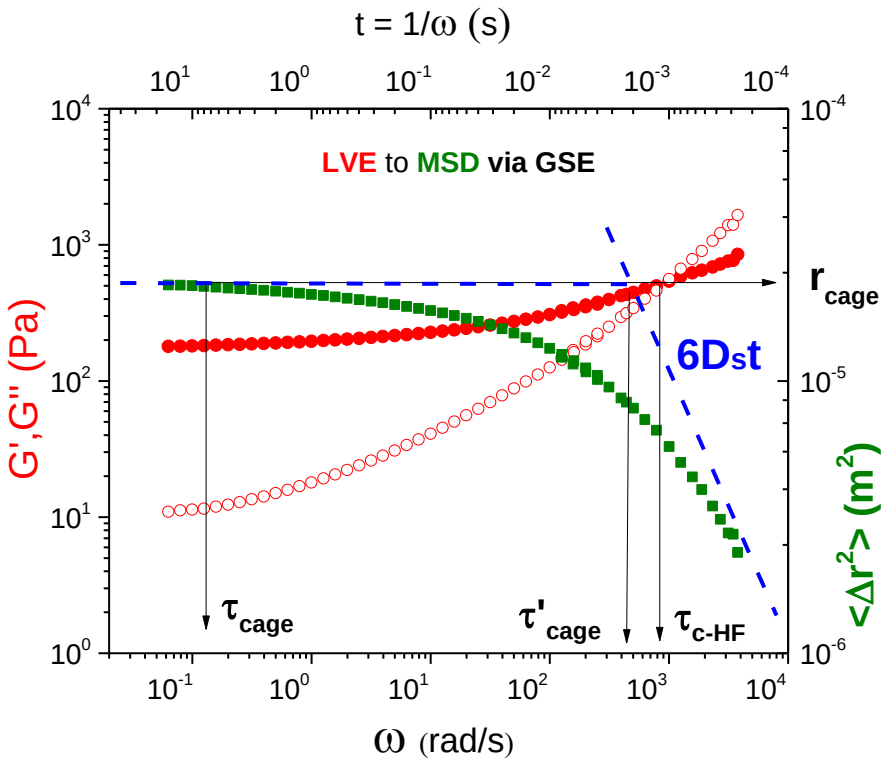

Fig. 1 Typical LVE spectrum (left Y axis), G′ (solid circles) and G′′ (open circles) of a colloidal glass at the HF regime measured with a commercial rotational rheometer MCR702 and a homemade PZR up to the angular frequency of 4000 rad/s. The corresponding MSD (right Y axis, solid squares) is obtained by rearranging Eq. (2) and (3). Abscissa is either angular frequency (bottom) or the corresponding observation time t = 1/ω (top). An indication of the dynamic cage size, r_{cage} can be provided by the MSD plateau. The corresponding times for the high frequency cross-over and approach to the cage limits are also indicated by the vertical arrows.

Fig. 1 presents the interrelation, via equations 1-4, of a measured LVE spectrum to the corresponding particle MSD for a hard sphere colloidal glass. The sample used as an example here is a suspension of PMMA particles of hydrodynamic radius R_h = 151 nm in a viscous solvent (squalene) with a volume fraction ϕ = 0.63. At long times (low frequencies) particles are localized within a cage localization length, r_{cage}, determined by the plateau of the MSD. This localization length is linked to the plateau modulus of G′via the GSE relation. At short times (high frequencies) the MSD slope approaches a linear dependence on time. The corresponding volume fraction dependent short-time diffusion coefficient, $D_s(\phi)$, at such high volume fractions, is expected to be about one order of magnitude slower than the dilute suspension (bare) SE diffusion coefficient, D_0. A localization time is defined as the time required for a particle to sufficiently explore its environment i.e. to “feel” its cage constraints and become transiently localized by its nearest neighbors. This process represents a transition of the MSD from diffusive to highly sub-diffusive,

View Article Online
DOI: 10.1039/D4SM01428F

and the corresponding localization time can be *crudely estimated* as $\tau'_{cage} = r_{cage}^2 / 6D_s(\phi)$, where r_{cage} is the displacement related to the dynamical cage size, as defined by the MSD long-time plateau. Still particles need, on average, significantly longer time to reach a distance equal to r_{cage}; this time was qualitatively introduced above and is indicated as τ_{cage} in Fig. 1. From this simple graphical representation, it is clear that this microscopic localization time τ'_{cage} and the $\tau_{c\text{-}HF}$ deduced from macroscopic linear viscoelastic measurements at the high frequency $G' = G''$, cross-over point, are comparable and potentially interrelated.

We should point out here that the microscopic dynamics deduced from the high frequency LVE measurement (shown in Fig. 1) could in principle be measured by optical microscopy or dynamic light scattering (DLS), when the latter probes, under certain contrast conditions, the self intermediate scattering function and therefore particle self-diffusion. In that sense hydrodynamic effects present in quiescent colloidal systems, affect the dynamics probed both in LVE and DLS in the same way. On the other hand, under non-linear shear (not utilized here), hydrodynamic interactions would strongly affect the microstructure and microscopic dynamics.

3. Nonlinear Langevin equation theory

Within the dynamical, "ideal" MCT, glass transition picture for hard sphere colloidal glass formers, the long-time diffusivity, $D_L(\phi)$, approaches zero experimentally at $\phi_g \sim 0.58$ for monodisperse spheres. This is typically only inferred via an extrapolation from experimental and simulation data by fitting to a presumed functional form, e.g., the critical inverse power law of MCT. On the other hand a finite slow α-relaxation has been detected at higher volume fractions of slightly polydisperse particles where it is argued the α time crosses over to an activated form (30,45). In contrast to this "ideal" MCT glass transition picture, the Nonlinear Langevin Equation (NLE) theory predicts a non-zero D_L up to ϕ_{RCP}. This is due to the thermally activated hopping of particles over an entropic barrier (computed microscopically) that always restores ergodicity via cage escape, in principle, at long enough times (46). This is qualitatively consistent with experimental observations (43) for the out-of-cage diffusion which is predicted to freeze only at RCP, avoiding MCT singularities which have been estimated by various methods to lie in the interval $0.64 >> \phi > 0.515$. The precise value of the latter number depends on structural input to MCT and the statistical mechanical level of a MCT-like analysis (47,47) employed, but is always below RCP. The short-time diffusivity, $D_s(\phi)$ remains finite and measurable even upon

View Article Online
DOI: 10.1039/D4SM01428F

approaching $\phi_{RCP} \sim 0.64$ for monodisperse spheres due to local in-cage particle diffusion since some internal free volume is still available.

Within NLE theory, the entropic barrier emerges from the prediction of a spatially-resolved effective dynamic free energy, $F_{dyn}(r)$, where r is scalar particle displacement from its initial position, and the negative gradient of the dynamic free energy defines an effective force on a particle due to all surrounding particles. It is calculated based solely on equilibrium structural input via the radial distribution or pair correlation function, g(r), or its Fourier analogue, the static structure factor S(q) (40,41), and is given as

$$\beta F_{dyn}(r) = -3ln\left(\frac{r}{d}\right) - \frac{1}{(2\pi)^3}\int dq \frac{\rho C^2(q)S(q)}{1+S^{-1}(q)} e^{-q^2r^2[1+S^{-1}(q)]/6} \quad (5)$$

Here, d is the particle diameter, $\beta=1/k_BT$ the inverse thermal energy, C(q) is the Fourier transform of the direct correlation function C(r), $S(q)=\left(1-\rho C(q)\right)^{-1}$, and ρ the particle number density. An example of the dynamic free energy for $\phi = 0.58$ is shown in Fig. 2(a). It consists of an ideal entropy-like term, which favors the "delocalized" Fickian diffusion liquid state (per the $-3ln\left(\frac{r}{d}\right)$ term in Eq. (5)), and a smoothly decaying, negative contribution, finite at r = 0 (the second term in Eq. (5)) due to interparticle interactions and correlations which favors particle localization. The minimum of the dynamic free energy defines a simple measure of the transient localization length r_{loc} in the cage. The combination of the two contributions in Eq. (5) leads to an entropic (for hard spheres) activation barrier in dimensionless units, βF_B (see Fig. 2(a)), beyond a volume fraction of ~0.43 that must be surmounted via thermally driven hopping to achieve out of-cage motion and ultimately structural relaxation and long distance Fickian diffusion. However, the barrier is only of order of k_BT or less until the volume fraction approaches the onset of the thermodynamically metastable regime at $\phi \sim 0.49$, and hence activated dynamics emerge only sufficiently deep in the metastable regime where the barrier is significantly higher than k_BT.

The required structural input (S(q) and c(q)) for hard sphere fluids in Eq. (5) can be calculated from the Ornstein-Zernike (OZ) integral equation (48):

$$h(r) = c(r) + \rho \int c(|r-r'|)h(r')dr' \quad (6)$$

where $h(r) \equiv g(r) - 1$, and an approximate closure relation needed. The classic Percus–Yevick (PY) is a good approximation in the normal fluid regime, but not nearly as accurate in the metastable regime of present interest since it sets c(r) to zero outside the hard core and misses important many

View Article Online
DOI: 10.1039/D4SM01428F

body effects (48). Recent combined theory and simulation work, for metastable regime, has shown that the Modified Verlet (MV) (49,50) closure is remarkably accurate up to very high volume fractions of ~ 0.585 (51). Physically, the key is that the direct correlation function has a short-range attractive tail outside the core that grows in amplitude with volume fraction (see Fig. 2(b)). This effective many body attraction strongly modifies g(r) and S(q), the key input to the dynamical free energy construction in NLE theory.

The OZ-MV theory for monodisperse hard sphere fluids predicts a structural and thermodynamic crossover at ϕ_s~0.60 associated with new type of many body effects (52). The distinctive changes of all equilibrium properties are in good accord with simulations and experiments, (52). As true of all approximate integral equation theories, the location of RCP is not captured correctly and is typically (well) beyond 0.644. For the OZ-MV theory, it is found at ϕ_{RCP}~0.77. Though far beyond the correct value of 0.644, it is much closer to the correct value than well studied integral equations theories such as OZ-PY, or popular empirical representations such as the Carnahan-Starling model, which both locate the incompressible RCP state at ϕ=1. Moreover, it has been argued the new physics that emerges in the deeply metastable state (e.g. ϕ>0.60) but well below the RCP volume fraction is not affected to leading order by the too large value predicted for ϕ_{RCP} (52).

Given the dynamic free-energy from Eq. (5), the mean time required for a tagged particle to displace "downhill" from its initial position to the minimum (localized state) in the overdamped limit (no inertia) can be computed by using Kramer's mean first passage time theory (53,54) as

$$\frac{\tau_{loc}}{\tau_0} = \frac{2g(d)}{d^2} \int_0^{r_{loc}} dr e^{F_{dyn}(r)/k_BT} \int_0^r dr' e^{-F_{dyn}(r')/k_BT} \quad (7)$$

where g(d) is the value of the radial distribution function at contact (d = 2R) and it enters via quantification of the short time dissipative friction relevant to hard sphere colloidal suspensions (40,55). Eq. (7) ignores collective elastic contributions to the barrier of ECNLE theory (56,57) which have been shown to be critical for the deeply metastable regime alpha time which is associated with the relatively large particle displacements characteristic of barrier crossing. However, this long-time contribution is not important for the present analysis of the dynamic elastic shear modulus and localization length on short-time and -length scales. The dynamically relaxed elastic shear modulus plateau associated with the transiently localized state can then be

View Article Online
DOI: 10.1039/D4SM01428F

calculated theoretically by projecting stresses onto collective density fluctuations in the usual way, and within the single particle dynamical framework of naïve MCT (NMCT) (58) one has:

$$G' = \frac{k_B T}{60\pi^2} \int_0^\infty dq \left[q^2 \frac{d}{dq} ln\big(S(q)\big) \right]^2 exp\left[\frac{-q^2 r_{loc}^2}{3S(q)}\right] \quad (8)$$

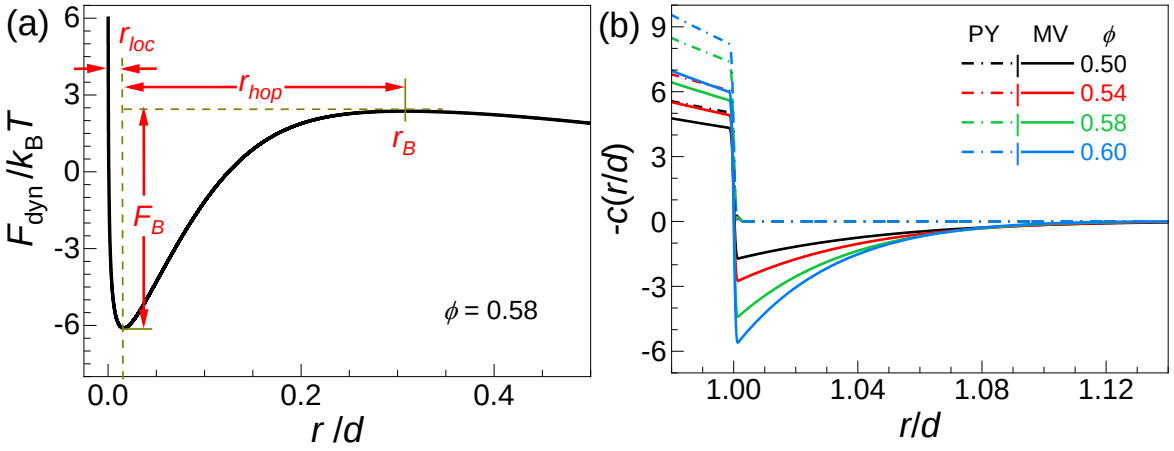

Fig. 2 a) Dynamic free energy in units of the thermal energy at $\phi = 0.58$. Localization and hopping jump lengths related to in- and out of-cage motion, respectively, are indicated, and F_B is the entropic barrier. b) Value of the direct correlation function with reversed sign for different volume fractions based on PY (dash-dotted) and MV (solid) closures in the near contact region. It represents an effective or renormalized interparticle interaction pair potential in units of the thermal energy.

We note that the mean-time scales for particle displacement to longer distances can be similarly computed. For example, though not our focus here, for the barrier crossing event identified as the elementary step of the long-time α-relaxation, the timescale follows from Kramers theory by changing the upper limit of the integration range from r_{loc} to the barrier location r_B as shown in Fig. 2(a), and including the collective elastic barrier contribution (56,57).

4. Materials and experimental methods

Sterically stabilized nearly hard-sphere PMMA particles with hydrodynamic radius R_h = 264 nm dispersed in squalene (Sigma Aldrich, Germany) were utilized as the primary sample. Steric stabilization is realized by chemically grafted poly-hydro-stearic acid chains (≈10 nm). Squalene was chosen as a solvent for its high boiling point and its refractive index proximity to PMMA in order to prevent evaporation and minimize any remaining Van der Waals attractions, respectively. Its relatively high viscosity enhances torque signal but most importantly slows down the in-cage dynamics allowing the high frequency crossover to be accessible to conventional

View Article Online
DOI: 10.1039/D4SM01428F

rotational rheometers such as MCR501, MCR702 (Anton-Paar, Austria) and ARES (TA Instruments, USA) and, our in-lab developed high frequency piezorheometer (PZR). MCR702 was fitted with cone–plate geometry and utilized in a separated motor transducer mode to minimize tool and sample inertia effects (39). The solvent shear viscosity was measured with a DMA 4100M viscometer (Anton Paar, Austria) and found to be η_s = 13.32 mPa s at T = 23 ^{o}C. The particle hydrodynamic radius was confirmed by dynamic light scattering measurements in the dilute regime.

Size polydispersity (standard deviation over the mean) of our samples is around 10% which suppresses crystallization. Different volume fractions were prepared from a single random close packing (RCP) batch, created by centrifugation. Starting from RCP, which was taken to be $\phi_{RCP} \approx$ 0.67 (for a 10% polydisperse particles) (59) the sample was successively diluted from about 0.64 to 0.45, with a total of 38 discrete samples progressively prepared, ensuring an accurate determination of the volume fraction among each other and relative to the initial RCP sample. More recent work (60) suggest that the RCP volume fraction for 10% polydisperse hard spheres is in the range 0.638-0.658 depending on compression rate (or centrifugation speed in our experimental protocol), i.e. clearly lower than that estimated by Schaertl et al. (59) which we use in this study, for consistency with our previous work (25).

Aging at these systems is weak and affects mainly G´´ at the lower frequency-end as short time in-cage dynamics are essentially age-independent (39,61,62); hence the system is considered within the experimental timescales as time invariant. Particle swelling can induce significant uncertainties and therefore the stock sample was left at rest for two months after solvent exchange and then centrifuged to RCP. After solvent addition the vial was placed on a rolling mixer for sufficiently long period depending on the concentration. Once particle dispersion was completed, followed by a rest time of 12 hours, the sample was loaded on the rheometer. A reduction of the rest time was required for the less concentrated samples ($\phi < 0.58$) to prevent sedimentation. All measurements were completed within 2 hours upon loading with no shear induced rejuvenation, i.e. no steady or oscillatory pre-shear.

To accurately determine the HF moduli crossover small amplitude oscillatory shear measurements were performed with 20 points per decade in the frequency regime of interest. Each dynamic frequency sweep measurement was performed at the optimum strain amplitude (ranged from 2% to 0.8%) in order to achieve significant torque signal and keep perturbation below the

View Article Online
DOI: 10.1039/D4SM01428F

linear limit determined by dynamic strain sweep. A weak evolution of the moduli was observed in very dense samples ($\phi > 0.6$) within the first 30 minutes. At longer times the LVE spectra and particularly the HF crossover were found to be time independent. Plate-plate 25 mm geometry was utilized in the very dense samples to overcome difficulties related to loading a stiff sample. Less concentrated samples were measured with cone – plate 50 mm geometry in the ARES rheometer.

5. Results and discussion

Dynamic frequency sweeps were utilized to capture the LVE spectrum of these hard spheres suspensions as volume fraction is systematically decreased. The angular frequency and modulus of the HF crossover were the parameters of specific interest. Hence, the conventional MCR702 or ARES data were complemented by measurements in the PZR when needed, i.e., at very concentrated samples where the HF crossover is detected at higher frequencies, beyond the range of conventional rheometers.

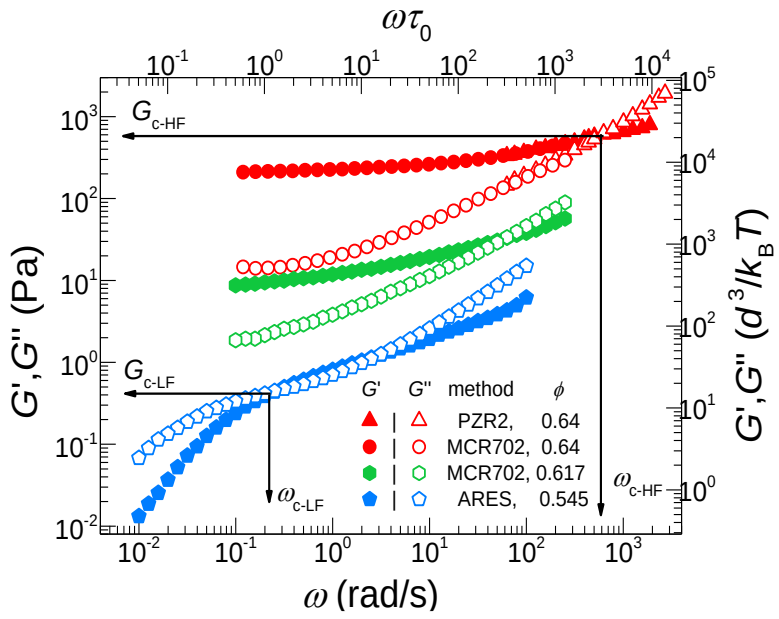

Fig. 3 Dynamic frequency sweeps of concentrated (ϕ=0.64, 0.617 and 0.545) hard spheres (R_h = 264nm) dispersed in squalene at T = 23°C. Measurements were performed by various commercial rotational rheometers such as MCR 702, ARES and, our in-lab developed PZR as indicated. Vertical and horizontal arrows point to the dynamic moduli crossover frequency, ω_c, and modulus (magnitude), G_c, respectively.

The LVE spectra of three samples (out of the total 38 measured) are shown in Fig. 3. The most concentrated sample with ϕ = 0.64 exhibits the HF crossover at 586 rad/s while at lower frequencies the caging plateau emerges. As ϕ is decreased to 0.617, still in the nonequilibrium

View Article Online
DOI: 10.1039/D4SM01428F

glassy regime, $\omega_{c\text{-}HF}$ decreases and falls within the frequency range of the MCR702 instrument. This frequency decrease of the HF crossover reflects the cage enlargement and the less frequent exploration of cage boundaries exhibited by the particles as their concentration is reduced. The caging plateau is shifted to even lower frequencies with no indication of a LF crossover at the lower frequencies reached, (0.1 rad/s). On the contrary, at $\phi = 0.545$ the LF crossover becomes faster and the HF crossover slower, and hence both are now accessible with our conventional rotational rheometers. In this low volume fraction but still in the metastable regime, the cage becomes larger and weaker as the entropic barrier height decreases resulting in more frequent out-of-cage hopping events.

Short-time dynamics: theory and experiment

Kramers' theory is used to predict the mean first passage time for a particle to displace "downhill" on the dynamic free energy from r = 0 to r_{loc} (see Fig. 2(a) and Eq. (7)) and thereby reach its transiently localized state (40) and become "caged", thereby defining the localization time, τ_{loc}. The theoretical predictions can be compared with the experimental time (or frequency) of the HF crossover obtained from LVE measurements. This comparison is shown in Fig. 4 where the behavior of $\omega_{c\text{-}HF}$ for the entire ϕ range probed (panel (a)) and the NLE theory predictions for $\omega_{loc} = 1/\tau_{loc}$ from Eq. (7) (panel(b)) are depicted. Interestingly, our experimental results reveal *two* exponential regimes with a much stronger exponential increase at ultra-high volume fractions. In particular, the experimental data for $\phi > 0.60$ show an exponential increase as $\omega_{c\text{-}HF} \sim \exp(61\phi)$, while for lower volume fractions (still high in an absolute sense) the slope is a factor of 2 smaller, per $\omega_{c\text{-}HF} \sim \exp(31\phi)$. Data enclosed in the dashed rectangle, corresponding to the even lower volume fraction regime ($0.53 < \phi < 0.55$), depart from $\exp(31\phi)$ behavior, and will be discussed later.

The NLE theory predictions for monodisperse hard sphere fluids in Fig. 4(b) for the localization time τ_{loc} are expressed in units of the elementary bare timescale, which, as discussed above, for a colloidal suspension is $\tau_0 = R^2/D_0$ with D_0 the dilute suspension Stokes-Einstein diffusion constant. Results are plotted as the dimensionless $\omega_{loc} = 1/\tau_{loc}$, and are in good semi-quantitative accord with the experimental data. In particular, the two exponential behaviors are predicted, and the ratio of the exponential slope parameters are comparable to that of the experimental data (a factor of ~ 2), albeit smaller in an absolute magnitude sense. Moreover, the absolute value of ϕ at the crossover between the 2 exponential regimes is nearly the same for theory

View Article Online
DOI: 10.1039/D4SM01428F

and experiment, occurring at a value of $\phi \sim 0.6$. Notably, this change of slope only appears when the structural input to NLE theory is from OZ-MV theory, as indicated by the black squares in Fig. 4(b). Moreover, the exponential growth laws have a theoretical basis in OZ-MV theory which predicts multiple structural metrics (including the density correlation length objectively deduced from h(r)=g(r)-1) to grow exponentially in the metastable regime (63). On the other hand, the dynamical predictions that use OZ-PY theory structural input in Fig. 4(b) (purple circles) exhibit a single exponential regime, a direct reflection of the absence of the new emergent many-body attraction in the direct correlation function in OZ-PY theory (52). Thus, the crossover of the two exponential regimes observed in experiments is attributed to the importance of the new structural many-body effects on the dynamic caging process that leads to particle localization in the highly dense metastable or so-called deep glass state.

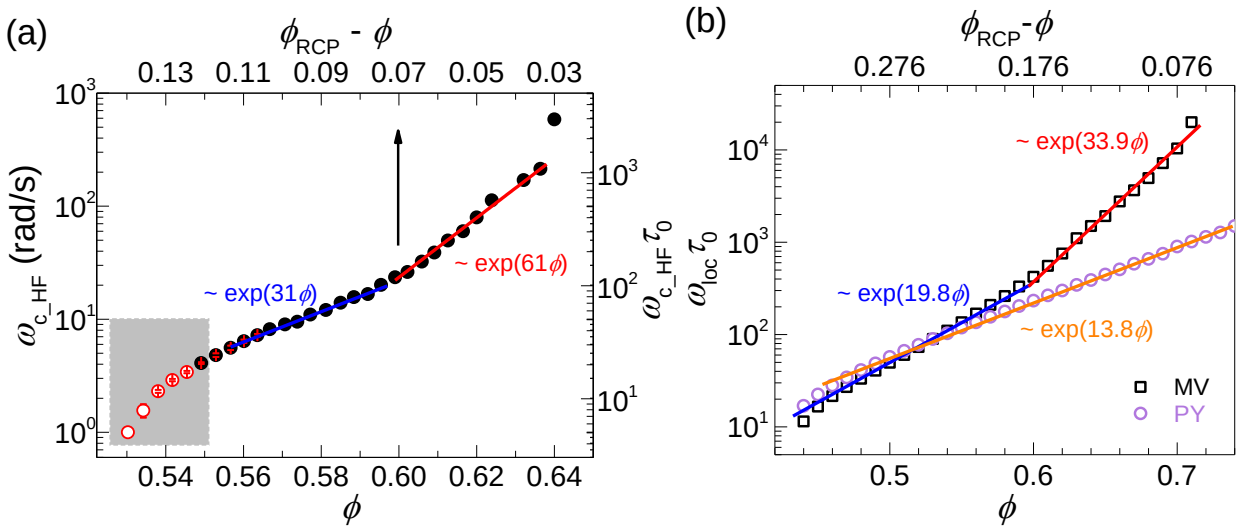

Fig. 4 Volume fraction dependence of a) the HF crossover frequency obtained from small amplitude oscillatory shear experiments scaled by the bare Brownian time ($\tau_0 = R^2/6D_0$) (right axis) and unscaled (left axis) and b) the dimensionless localization frequency (τ_0/τ_{loc}) related to the in-cage dynamics calculated from NLE theory (Eq. 7) with MV closure approximation (open squares) and PY closure (open circles), where the y-axis (ω) is also normalized by τ_0. The lines in both (a) and (b) indicate the different slopes as denoted. The vertical arrow in (a) indicates the experimental distance from RCP for the critical volume fraction for change of slope. Data points in (a) shown in open red symbols (shaded area) are discussed below in Fig. 8. The top horizontal scale in panel (b) indicates the distance in volume fraction from the OZ-MV theory predicted RCP volume fraction.

View Article Online
DOI: 10.1039/D4SM01428F

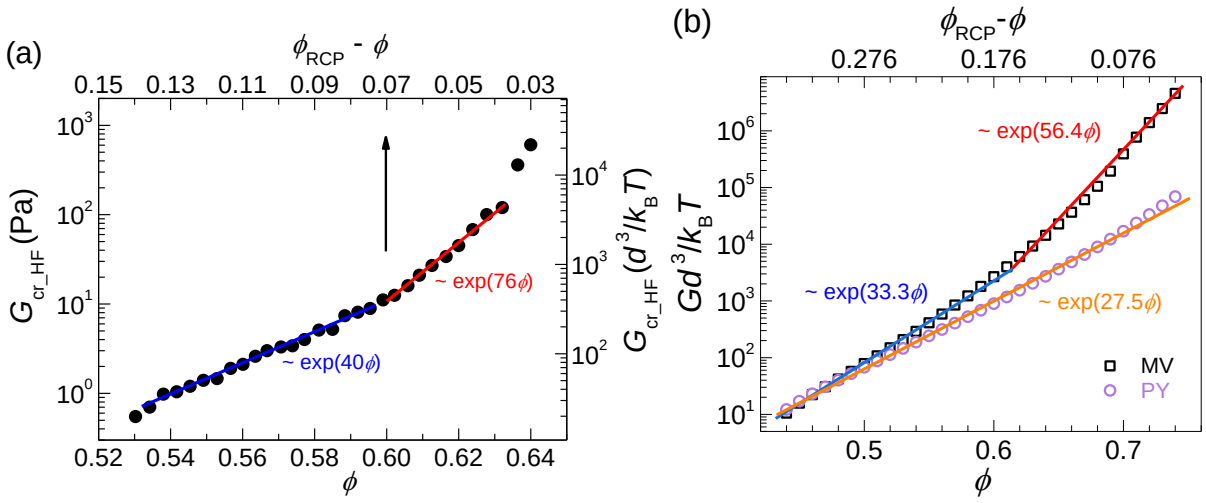

Fig. 5 Volume fraction dependence of a) the HF crossover modulus obtained from experiments with hard spheres, R_h = 264nm dispersed in squalene at T = 23°C and b) the normalized elastic shear modulus calculated theoretically from Eq. (8) with MV closure approximation (open squares) and PY closure (open circles), where the y-axis is normalized over thermal energy per volume to allow comparison with theory. The lines indicate the different slopes as in Fig. 4. The vertical arrow indicates in (a) the experimental distance from RCP at the critical volume fraction where data exhibit a change of power law slope. The top horizontal scale in panel (b) indicate the distance in volume fraction from the OZ-MV theory predicted RCP volume fraction.

The theoretically predicted $G_{c\text{-}HF}$ corresponds to the value of the elastic shear modulus in the localized state and is computed using Eq. (8). This is effectively a MCT calculation albeit within the simpler single particle based "naïve" version (52). The theoretical dynamic shear modulus also exhibits two regimes with a change in slope at ϕ = 0.6, consistent with the experimental findings, as shown in Fig. 5. This qualitative behavior has been observed in earlier work (25) and attributed to a rheological signature of the glass transition that was shifted to higher volume fraction (compared to the nominal at $\phi \approx 0.58$) due to particle polydispersity. The present theory clearly predicts the same behavior for monodisperse spheres if the effective many body attractions in c(r) contained in the MV closure are included. Therefore, the two exponential regimes in $G_{c\text{-}HF}(\varphi)$ and $\omega_{cr\_HF}(\varphi)$ observed experimentally are again a consequence of the importance of many-body effects in local packing structural correlations and elastic stress storage which is strongly coupled to slow density fluctuations. This implies that these many body interactions, though not negligible at ϕ smaller but close to 0.6 (see Fig. 2(b)), become very important at higher volume fractions, and dominate at $\phi > 0.6$ (see Fig. S1).

View Article Online
DOI: 10.1039/D4SM01428F

If the experimental and theoretical results in Fig. 4 and Fig. 5 are compared quantitatively then one should note that the shear modulus results of the latter have been extended to higher volume fractions (up to about 0.72). This high value (for all integral equation theories) is still well below the RCP volume fractions predicted by OZ-MV theory as discussed above and in depth in ref.(52). We do not believe this caveat affects the model predictions at lower volume fractions, as has also been discussed in (52). Nevertheless, we also present in Fig. 4 and Fig. 5 both the experimental and theoretical data plotted as a function of the distance to their corresponding RCP volume fractions, even though we do not expect this distance is the controlling factor that determines the new physics for Brownian colloids. Indeed, we emphasize that the second exponential regime in G′ (as well as in the high cross over frequency) emerges from the theory well below the theoretical RCP. For the experiments, we note that although the absolute volume fraction values depend on the value of φ_{rcp} used, the relative distance to rcp, $\varphi_{rcp} - \varphi_s$, is not affected. Moreover, direct comparison of theory results for a monodisperse hard sphere model with the polydisperse colloid experimental system inevitably involves some (modest) quantitative uncertainty. It is to within these caveats that all quantitative comparisons of theory and experiment at a fixed common value of absolute volume fraction should be viewed.

Overall, we believe that our findings above contribute to a deeper understanding of the nature and origin of the dynamical cage concept as it relates to the correlated pair structure. One can identify a characteristic crossover volume fraction of $\phi \sim 0.6$ in the various dynamic properties (Fig. 4 and Fig. 5) as ϕ_s defined above based purely on a qualitative change of structure and thermodynamics in the deeply metastable regime, which signals when a new type of many body effects become dominant. This deduction relates to simulation findings that indicate, irrespective of the existence or not of an MCT-like glass transition volume fraction, the emergence of a distinct type of dynamic and structural response in a high volume fraction regime approaching RCP but well below it (52,64–66). On the experimental side, this volume fraction regime is identified with a type of nonequilibrium glassy state as defined in a practical sense where i) crystallization (if particles are monodisperse) is practically suppressed, ii) the α relaxation is long enough (though presumably not infinite) that is practically out of the experimental window (see extrapolation shown in Fig. S2), and iii) a solid like response is observed at all practical timescales. In colloidal suspensions, this volume fraction (usually denoted as ϕ_g) is typically estimated to be ~ 0.58-0.6,

View Article Online
DOI: 10.1039/D4SM01428F

with the exact value depending on particle polydispersity, compression rate, and/or other experimental or simulation conditions.

Returning to the primary issue of the relatively short time and length scale dynamics, an important question is whether there is any intuitive theoretical understanding of why ω_{loc} behaves so similarly to the dynamic shear modulus G in Fig. 5, a trend observed in our experiments. In order to provide an answer, we explore different technical simplifications of the NLE theory since we do not directly theoretically analyze the frequency-dependent moduli. First, we note that the theoretical result for $\omega_{\mathrm{loc}}\tau_0$ in Fig. 4(b) was numerically calculated based on Eq. (7) with specific input from the dynamic free energy of Eq. (5), an approach we call Method-I. As discussed above in the theoretical background section, $F_{\mathrm{dyn}}(r)$ contains two contributions, one favoring delocalization, and one favoring localization, and both are included in Method-I. Regarding the short-time and -length scales associated with particle displacements that reach the localized caging state, activated barrier crossing processes are entirely irrelevant, suggesting the first contribution might dominate to leading order. One can thus simplify the dynamic free energy to $\beta F_{\mathrm{dyn}} \cong -3ln\left(\frac{r}{d}\right)$. Substituting this in Eq. (7), and employing the correctly computed value of r_{loc} from the full theory, one can obtain a different estimate of $\omega_{\mathrm{loc}}\tau_0$, an approach we call Method-II. A third approach follows from noting that the dynamic free energy near its minimum is, by definition, parabolic, per an Einstein amorphous solid. This suggests considering the harmonic approximation $\beta F_{\mathrm{dyn}} = \frac{K_0}{2}(r-r_{loc})^2$ where the spring constant K_0 is the curvature at the localization length scale r_{loc} predicted by the full NLE theory, an approach we call Method-III.

To test the robustness of our theoretical analyses, the results of these three different approximate Methods are compared in Fig. 6. We find that Methods II and III deliver very similar results as that shown in Fig. 4(b): two exponential regimes with the crossover at nearly the same volume fraction. Moreover, all slopes in the same ϕ range are nearly identical for all three Methods. This agreement provides support for the idea that, although the theory does not explicitly analyze the frequency dependent shear modulus, the extraction of related information from the dynamic free energy reports information physically akin to the experimental ω_{loc}, a conclusion in accord with our a priori physical expectations.

View Article Online
DOI: 10.1039/D4SM01428F

To test the level of quantitative agreement between the functional form of the predicted results based on the different methods, the results of Methods II and III are vertically shifted to align them with the predictions based on Method I. Encouragingly, the inset of Fig. 6 shows that a well-collapsed master curve is obtained. Thus, the short time or high frequency behavior associated with cage formation and the onset of particle location discussed in Fig. 4(a) from experiment, and in Fig. 4(b) from the NLE theory, can be interpreted as corresponding to a physical picture of particle motion akin to a damped, Brownian, localized vibrational-like downhill motion. Finally, analytic insight can be obtained based on Method-II since the integral of Eq. (7) can be exactly performed thereby yielding $\omega_{\rm loc}\tau_0 = \frac{d^2}{2g(d)r_{loc}^2}$. This result provides explicit physical insight into what controls the inverse localization time: the dynamic localization length, and the contact value of g(r) which amplifies the pure solvent friction, ζ_{SE}, to that felt by a translating colloid in concentrated suspensions, ζ_s, due to independent binary collisions on short-length and -time scales (as $\frac{\zeta_s}{\zeta_{SE}} = g(d)$)(40). In addition, it has been well established previously, both numerically and analytically (58), that the dynamic elastic shear modulus within the NMCT framework is predicted to obey a microrheology-like relationship to the inverse square localization length r_{loc}^{-2}, per $\beta G d^3 \approx \frac{9}{5\pi}\frac{\phi d^2}{r_{loc}^2}$. Combining this with the above relation $\omega_{\rm loc}\tau_0 = \frac{d^2}{2g(d)r_{loc}^2}$, we obtain an interesting connection between shear modulus and short-time frequency as $\beta G d^3 \propto \phi g(d)\omega_{\rm loc}\tau_0$.

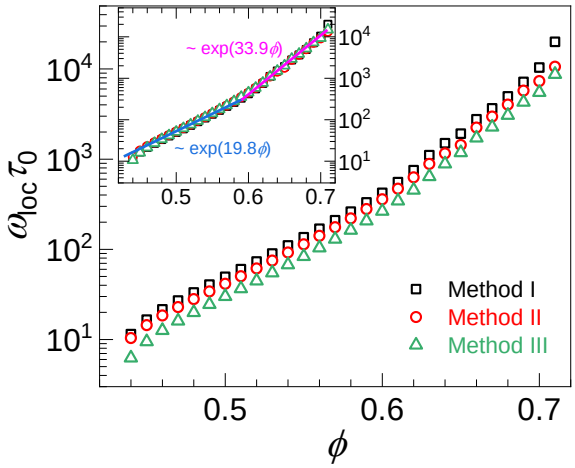

Fig. 6 Volume fraction dependence of the dimensionless localization frequency, $\omega_{\rm loc}\tau_0 \equiv \tau_0/\tau_{loc}$, based on the 3 theoretical Methods I, II and III described in the text. (Inset) Same display as in the main frame but with red and green data vertically shift up by a multiplier 1.25 and 1.7, respectively.

View Article Online
DOI: 10.1039/D4SM01428F

For further perspective, we note that in the framework of NLE theory, an analytic relationship between the localization length and the contact value $g(d)$ was deduced (58) as $\frac{d^2}{r_{loc}^2} \propto \phi^2 g^4(d)$. Combining this relation with the above results of $\beta G d^3 \approx \frac{9}{5\pi}\frac{\phi d^2}{r_{loc}^2}$ and $\omega_{\mathrm{loc}}\tau_0 = \frac{d^2}{2g(d)r_{loc}^2}$, we predict that both the elastic shear modulus and the short time dimensionless frequency $\omega_{\mathrm{loc}}\tau_0$ obey a power law relationship with the contact value $g(d)$. This is a physically appealing result given that the rate of collisions in a hard sphere fluid scales with the contact value, and that stresses in hard sphere fluids are associated with impulsive "forces" and hence particles being in contact. This consistency physically explains why $\beta G d^3$ and $\omega_{\mathrm{loc}}\tau_0$ behave so similarly in Fig. 4 and Fig. 5, e.g., slope change in the two exponential growth laws and crossover position.

Furthermore, by combining the above analytic relations we obtain $\beta G d^3 \propto \phi g(d)\omega_{\mathrm{loc}}\tau_0 = \phi^{0.33}(\omega_{\mathrm{loc}}\tau_0)^{1.33}$. Within the theory, this power law relationship between G and $\omega_{\mathrm{loc}}\tau_0$ is easy to test based on numerical calculations, as shown in Fig. 7(b), where one sees it works extremely well, although the power law exponent in numerical calculation is slightly larger, ~1.53. To validate this power law prediction further, we plot the HF crossover modulus obtained from experiments ($G_{cr\text{-}HF}$) as a function of the crossover frequency (ω_{cr_HF}) in Fig. 7(a). Remarkably the data do obey a power law relation with an exponent of 1.25, modestly lower than the numerically and analytically obtained values of ~1.53 and ~1.33, respectively.

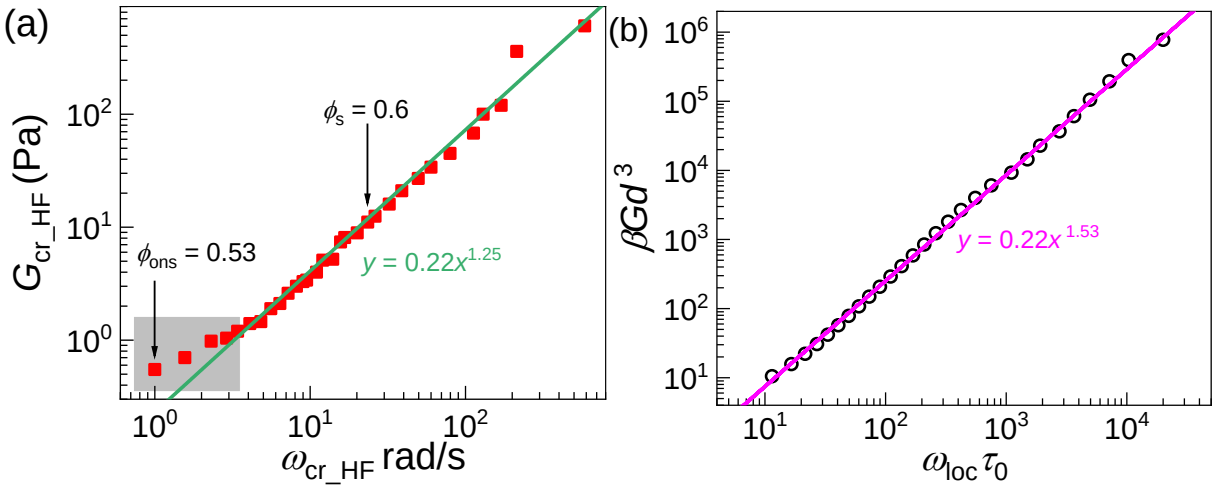

Fig. 7 Modulus at the high frequency crossover as a function of the corresponding frequency in (a) experimental (red solid squares) and (b) theoretical (black open circles) data. The plot verifies the theoretically inspired power law relationship between dimensionless shear modulus and $\omega_{\mathrm{loc}}\tau_0$. Solid lines indicate the power law fits with slope

View Article Online
DOI: 10.1039/D4SM01428F

values as indicated. Vertical arrows in (a) indicate the characteristic volume fractions, ϕ_{ons} and ϕ_{s}, discussed in the text. The shaded area in (a) indicates the lower volume fraction regime data shown also in Fig. 4.

Given the origin of the analytical theoretical relations deduced above, we suggest that they may be relevant to other spherical particle systems with different interparticle interactions, for example in dense suspensions sticky spheres and perhaps thermal liquids. However, it is often difficult to measure the contact value $g(d)$ experimentally for nanoparticle or colloidal fluids, and essentially impossible for thermal liquids. Moreover, strong repulsive intermolecular interactions are generally not literally hard core. In the latter case, one could replace $g(d)$ with the first maximum value of g(r). Future experiments can test the power law relationship of Fig. 7 in other complex systems such as viscous molecular liquids.

Long-time dynamics: experiment and theory

Contrary to the high frequency crossover, the LF crossover shifts to shorter times as volume fraction is decreased and hence becomes visible in the frequency range of the ARES rheometer, as shown in Fig. 8 for the volume fraction of 0.539. This shift is due to cage escape as these events become faster and more frequent. Consequently, as ϕ is decreased, the two crossovers tend to approach each other along the frequency axis until they merge. This behavior is in analogy with molecular glass formers, where the slow glassy α-mode and the more fluid-like β-mode timescales converge at sufficiently high temperature above the kinetic glass transition temperature (67).

The LF and HF crossover times and their merging point as derived from LVE measurements are shown in Fig. 9(a). For comparison, the short and long characteristic inverse times, $1/\tau_{\mathrm{loc}}$ and $1/\tau_{\mathrm{hop}}$ as calculated using Kramers mean first passage time theory within the NLE framework and which, as discussed above, arise from different parts of the spatially-resolved dynamic free energy, are also shown in Fig. 9(b). As mentioned earlier, the mean α process hopping time τ_{hop} is calculated from the same formula as the localization time (τ_{loc} in Eq. (7)) (68,69) but the integration range is from r_{loc} to r_{B} corresponding to the displacement required for the particle to surmount the entropic barrier in Fig. 2(a) per activated hopping dynamics. Indeed, the microscopic times τ_{loc} and τ_{hop} increase and decrease, respectively, with dilution until they become equal at $\phi \approx 0.43$, the NMCT transition point. At this volume fraction (merging point

View Article Online
DOI: 10.1039/D4SM01428F

derived from theory) the barrier approaches zero, and in its vicinity the barrier is less than k_BT and hence the idea of activated dynamics loses its physical meaning.

Overall, the theoretical results are in good agreement with the experimental observations considering the practical uncertainties stemming from aging of low frequency dynamics, ϕ determination, and errors associated to the measurement itself. We interpret this volume fraction deduced from the theory as defining the onset or emergence of dynamic caging, ϕ_{ons}. The corresponding experimentally-deduced value where the two cross-over frequencies merge takes place at around 0.53 (with distance from RCP, ϕ_{RCP}-ϕ = 0.14) for the present polydisperse sample. We note that this is comparable with the freezing volume fraction of 0.494 (where ϕ_{RCP}-ϕ = 0.146) for monodisperse hard spheres (70,71). Therefore, freezing as deduced from the experimental linear viscoelasticity data and the onset of cage formation volume fraction, ϕ_{ons}, as determined from the theoretical model, seems to coincide to leading order with the merging of the two characteristic times scales of the in-cage localization and out-of-cage escape.

We note that the merging point in the experimental and theoretical data takes place at similar, but not the same, volume fractions. The reason is well known, the NMCT predicts the dynamic crossover to activated motion at a quantitatively too low volume fraction due to its single particle nature. This theoretical point has been analyzed in great depth long ago (40,46). Moreover, the theory studies monodisperse hard spheres, while the experiments employ polydisperse samples which generically delay the emergence of slow dynamics to higher volume fractions. From the NLE perspective, for ϕ lower than the crystallization volume fraction the hard sphere suspension behaves in a more liquid-like manner since activated caging effects are not really important because the entropic barrier is only of order the thermal energy or less. In this regime, the non-self-consistently determined (55) friction associated with independent binary collisions and weak-caging are dominant. By the same token, from the theoretical perspective ϕ_{ons} marks a dynamic crossover that signals the onset of a barrier larger than k_BT, and a nontrivial separation of the minimum and maximum values of the dynamic free energy. Hence, this is the minimum volume fraction where short- and long-time dynamics begin to be separated by a caging plateau-like feature, although in practice clear observation of such a separation requires a barrier well beyond 1-2 k_BT, and hence a volume fraction beyond 0.5.

Below, but still near, ϕ_{ons}, experiment and theory agree that a continuous relaxation is observed, with short and long-time diffusion still distinguishable but not well separated by a clear

View Article Online
DOI: 10.1039/D4SM01428F

caging plateau. Moreover, D_s and D_L are comparable (although not identical) and affected by a binary collisions, hydrodynamic effects, plus the non-self-consistent weak-caging friction effects discussed above (55). Samples with volume fractions lower than ϕ_{ons}, such as the sample with ϕ = 0.449 in Fig. 8, exhibit no moduli crossover, i.e. they behave in a liquid-like manner with G´´ > G´ at all timescales. Nevertheless, despite the absence of a moduli crossover, the LVE spectrum is not featureless; the moduli approach more at a certain frequency where tan(δ) attains a minimum value (see Appendix A.2). This frequency seems to set a time scale with a different volume fraction dependence than the moduli crossover frequency above ϕ_{ons}. In this regime there is a "loose caging" effect imposed by neighboring particles; constraints are very weak, with barrier below 1 k_BT, and this is reflected in the dynamics with an absence of the typical caging plateau but still a clear separation of short and long diffusivity. At much lower volume fractions (not probed here) D_s and D_L approach each other and eventually at the dilute limit become equal to its bare value, D_0.

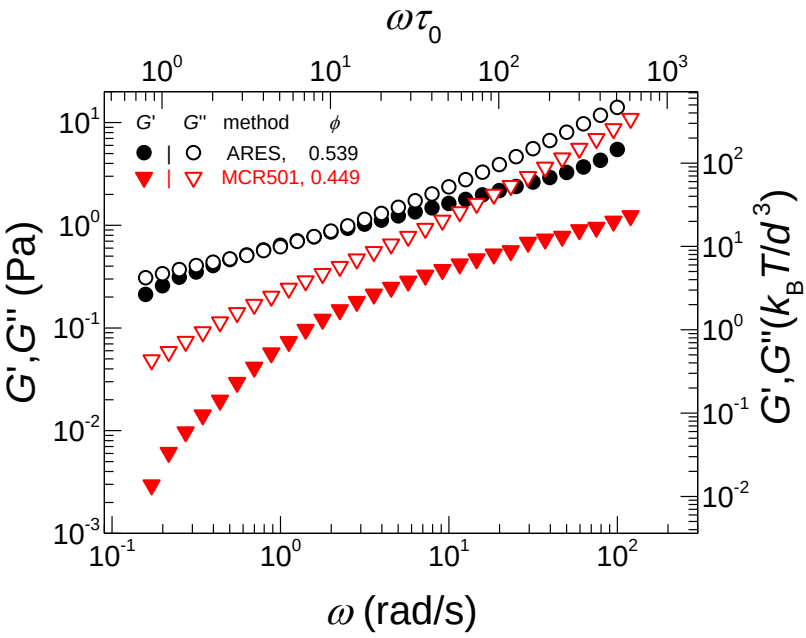

Fig. 8 Dynamic frequency sweeps of two less concentrated samples with ϕ = 0.539 and ϕ = 0.449 exhibiting moduli crossover and tanδ minimum, respectively. Particles are PMMA hard spheres of radius R_h = 264 nm dispersed in squalene at T = 23 °C. Measurements were performed using the MCR 501 and ARES rheometers.

View Article Online
DOI: 10.1039/D4SM01428F

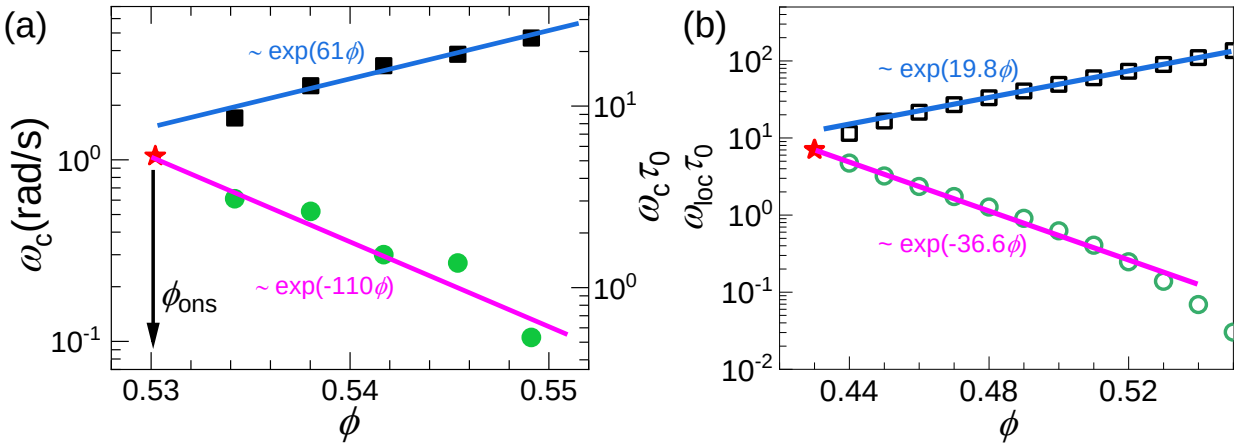

Fig. 9. Experimental LVE data (a) and the corresponding theoretical calculation (b) of the convergence of short- and long-time characteristic dynamical frequencies as a function of volume fraction. Circles denote the LF and squares the HF crossover frequency, respectively. Lines represent the exponential dependencies indicated. Red stars indicate the merging point of the two crossover frequencies. Vertical arrows indicate the merging point volume fraction ϕ_{ons}, which is found from experiment and theory to be $\phi \approx 0.53$ and $\phi \approx 0.43$ respectively.

In addition to the near quantitative agreement of experiment with NLE theory predictions for the volume faction dependence of the high frequency cross-over, $\omega_{c\text{-}HF}$, and corresponding elastic modulus $G_{c\text{-}HF}$ (Fig. 4 & 5), similar agreement between experiments and theory is observed for the approach of the frequencies $\omega_{c\text{-}H}$ and $\omega_{c\text{-}LF}$, identified with model predictions for $1/\tau_{loc}$ and $1/\tau_{hop}$ respectively. As seen in Fig. 9, these follow an exponential increase ($\omega_{c\text{-}HF}$ or $1/\tau_{loc}$) or decrease ($\omega_{c\text{-}LF}$ or $1/\tau_{hop}$) as a function of ϕ with larger exponents (as in the case of G'), higher for the LF (long -time hopping relaxation) than the HF (short-time cage localization time), and different in absolute values in experiment and theory. Interestingly we find out that the LF-to-HF exponent *ratio* of roughly a factor of two (110 : 61) observed in experiments is in good accord with that predicted by theory (36.6 : 19.8).

6. Conclusions

The characteristic time scales derived from the experimental G′and G′′ data dynamic crossovers at high and low frequencies of very dense hard sphere like colloidal suspensions have been determined for an extensive range of volume fractions. Overall, very good qualitative (and in some cases near quantitative) agreement of the distinctive trends is found with the predictions of the microscopic NLE theory, based on the spatially-resolved dynamic free energy concept. The characteristic frequencies exhibit a double exponential increase with volume fraction with semi-

View Article Online
DOI: 10.1039/D4SM01428F

quantitative agreement between experiments and theory. Two distinct volume fractions have been identified as ϕ_{ons} and ϕ_s. The former, $\phi_{ons,}$ signals the merging point of short- and long-time dynamics and, marks the onset of activated caging at a volume fraction of about 0.53 in the present polydisperse particle experiments. As expected, this value lies above that predicted by the single particle dynamics NLE theory for monodisperse hard sphere fluids. The ϕ_s is derived in experiments from the change of slope in the volume fraction increase of $\omega_{c\text{-}HF}$ or $G_{c\text{-}HF}$. It can be identified as an experimental dynamic crossover volume fraction that is connected theoretically with the emergence within OZ-MV theory of a new type of structural many-body effect as manifested in an effective attraction in the direct correlation function, c(r). Both the NLE theory and experiments agree that the dynamic crossover for $\omega_{c\text{-}HF}$ and $G_{c\text{-}HF}$ takes place at $\phi \sim \phi_s = 0.6$. A caveat is that this quantitative agreement should be taken cautiously given that the theory analyzes monodisperse hard sphere fluids while the experiment studies polydisperse colloidal suspensions. Overall, the experiments and theory indicate the existence of a regime above ϕ_s with a distinct character than that of the modestly metastable fluid below ϕ_s, which is crucial at very high volume fractions in determining the formation of a long-lived cages with implications for the microscopic dynamics and linear rheology. Experimentally this is identifiable with the non-equilibrium glass in the sense that the viscoelastic response is solid like at all finite frequencies probed. On the theoretical side it is linked to distinct dynamic, structural and thermodynamic behavior predicted to emerge in the equilibrated deeply metastable (or "deep glass") regime associated with new many body packing effects. Thus, the question of whether ϕ_s can be identified with the experimentally-deduced kinetic glass transition volume fraction ϕ_g where hard sphere suspensions are expected to transit to an effectively arrested state, and whether this is indeed identical in an observable properties sense to the equilibrated deep glass regime analyzed by the theory, remains open.

What is new in our modeling is the application of NLE theory with the accurate MV (rather than the PY) closure employed for the required structural input to make predictions consistent with our new experimental findings based on a wide volume fraction range, robust experimental data. One can also argue that this agreement provides additional new support for the dynamic free energy concept at the heart of NLE theory (which to date has focused on longer time and length scale processes than those studied here), and the important structural many body effects captured by the MV closure which are critical for quantifying dynamic caging constraints.

View Article Online
DOI: 10.1039/D4SM01428F

The presented new analytical theoretical results have also provided a microscopic physical basis for the mechanism of the experimentally observed nearly-identical behaviors of the high frequency (short time) localized dynamics timescale and the dynamic shear modulus. The physical picture is based on the small distance aspects of the spatially-resolved dynamic free energy, and is akin to dynamics describable as a damped, Brownian, localized vibrational-like "downhill" motion towards the transient localized state with the frictional resistance related to short time dissipative independent binary collisions.

Constraints by neighbors are evident in the rheological data at volume fractions below ϕ_{ons}. The frequency where the two moduli approach more ($\tau_{tan\delta}$ minima) sets a time scale, and hence provides important information that can be explored theoretically and experimentally in future work. In a similar manner, a systematic study of HF data of attractive glasses will provide insights on cage formation in the presence of competing attractive interparticle interactions and physical bond formation which reflects a rich interplay between entropic and enthalpic contributions in dynamic cage arrest. Further extension of the present work could aim to correlate ϕ_{ons} and ϕ_s with other characteristic volume fractions in glass forming suspensions (8) where it has been proposed that local domains of cooperatively moving particles become more rigid with increasing ϕ and eventually percolate leading to glassy, solid-like response. Overall, we anticipate that the data presented here, which were obtained by simple rheological experiments and interpreted in terms of NLE theory, will aid in developing a deeper understanding of the dynamical caging mechanism and the glass transition phenomenon.

Finally, we note that previous results based on ECNLE theory (63,72) showed that the mean α relaxation time of a deeply supercooled liquid (or metastable glass for hard spheres, ϕ>0.58) can be directly related to the dynamic shear modulus in an exponential manner. This result emerges from not only τ_{hop} involving the local cage barrier, but also inclusion of the longer range collective elastic barrier which is of critical importance. Combining this exponential behavior with the relationship found here between $1/\tau_{loc}$ and the dynamic shear modulus G′, an exponential connection between the mean α relaxation time and $1/\tau_{loc}$ is predicted. Most importantly, both the α relaxation time and the fast process relaxation rate $1/\tau_{loc}$ can, in principle, be measured experimentally over a wide range of degrees of metastability, which can provide an experimental test for the proposed exponential connection. This is of particular interest for supercooled thermal liquids where measurement of G′ at relatively high and intermediate temperatures is difficult.

View Article Online
DOI: 10.1039/D4SM01428F

Appendix A.1: High frequency scaling and volume fraction consistency

The weak power law dependence of G′ is sensitive to local interactions (Schroyen et al. 2019) and hence is strongly affected by the steric layer of colloids that induces deviations from ideal hard sphere interactions (73,74). The slope of G′ at frequencies above the HF crossover is typically 0.3 for hairy (sterically stabilized) particles (39,75). Furthermore, the volume fraction response of the total complex viscosity deduced at high frequencies can be used to determine the effective volume fraction of the suspension.

The uncertainties and the various methods of ϕ determination are well discussed in the literature (76). Given that all samples were prepared from the same initial batch by sequential dilution, the uncertainties in the relative ϕ are minimized. The reduced high frequency viscosity is given by $\eta'_{r,\infty}=\eta'_{\infty}/\eta_s$, where η_s = 13.3 mPa s for squalene at 23^0 C, and η'_{∞} is the limiting value of the real part of complex viscosity obtained from oscillatory shear. Once this is known, the theoretical volume fraction can be calculated (77,78) according to:

$$\eta'_{r,\infty}=15.78ln\left(\frac{1}{1-(\varphi/\varphi_{rcp})^{1/3}}\right)-42.47 \quad (9)$$

which is valid for $0.60 \leq \phi < \phi_{RCP} = 0.67$. The denominator portrays the singular behavior (divergence) of the high frequency viscosity at random close packing. This empirical equation is extended to ϕ as low as 0.6, a crossover point discussed in the main text, as the authors suggest a different equation for less concentrated regime (77). The calculated volume fractions from Eq. (9) and the experimentally estimated ones for four samples are summarized in table A1. Predictions from fitting using Eq. (9) are ~ 0.03 higher than the experimentally estimated values and in agreement with findings in our earlier work (39). The modest discrepancy could be attributed to our overestimation of η'_{∞} as the plateau value has not been fully attained (Fig. A1) or to particle polydispersity that would affect the quantitative accuracy of Eq. (9). However, the relative volume fractions are proven to be consistent. This indicates a reasonably good agreement of experimental data and theoretical predictions with a potential shift of experimental volume fractions by 0.03 would not significantly change any of the main findings of this work.

View Article Online
DOI: 10.1039/D4SM01428F

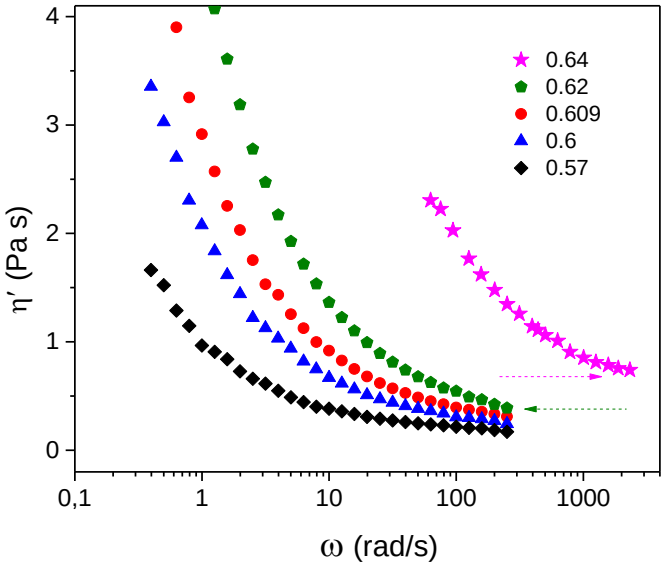

Fig. A1 The in-phase with strain rate dynamic viscosity limiting behavior of hard spheres, R_h = 264 nm dispersed in squalene at T = 23 °C. The legend indicates the experimentally estimated volume fraction. Data for ϕ = 0.64 (magenta symbols) are measured with PZR up to 3000 rad/s. Horizontal arrows indicate high frequency viscosity determination for the two highest volume fractions shown.

Table A1: Volume fraction of four samples: comparison of the experimental estimation with predictions of Eq. (9)

Determined from RCP	Prediction of Eq. (9)	Deviation
0.64	0.665	0.025
0.62	0.649	0.029
0.609	0.639	0.029
0.6	0.628	0.028

Appendix A.2: low volume fraction ($\phi < \phi_{ons}$) samples with no dynamic crossover

At volume fractions below ϕ_{ons} (~ 0.53 in experiments, see Fig. 8) the dynamic moduli do not exhibit a crossover, but they do approach each other at a certain frequency and this is clearly

View Article Online
DOI: 10.1039/D4SM01428F

detected as a minimum of tanδ=G´´/G´ as shown in Fig. A2(a). This frequency marks a time scale defined as $\tau_{tan\delta} = 1/\omega_{tan\delta}$. At this time scale the constraints felt by tagged particle due to its neighboring particles are maximized, and this can be viewed as a "loose caging effect". At shorter and longer times particle mobility appears higher. Interestingly, $\omega_{tan\delta}$ exhibits the opposite trend from $\omega_{c\text{-}HF}$ as shown in Fig. A2(b). This suggests that the characteristic time is related with the transition from in-cage (β-relaxation) to out-of-cage (α-relaxation) motion. Below ϕ_{ons} this is identified in experiments by $\tau_{tan\delta}$ increasing with φ, whereas above ϕ_{ons}, $\omega_{c\text{-}HF}$ is related with the time scale of cage exploration decreases with φ as shown in Fig. 8. Such non-monotonic behavior, with a maximum at ϕ_{ons}, is in reminiscent of the time scale τ_B determined from dynamic light scattering data (or from the self-intermediate scattering function) as the transition time scale between α and β-relaxations around the glass transition volume fraction by van Megen & Underwood (79).

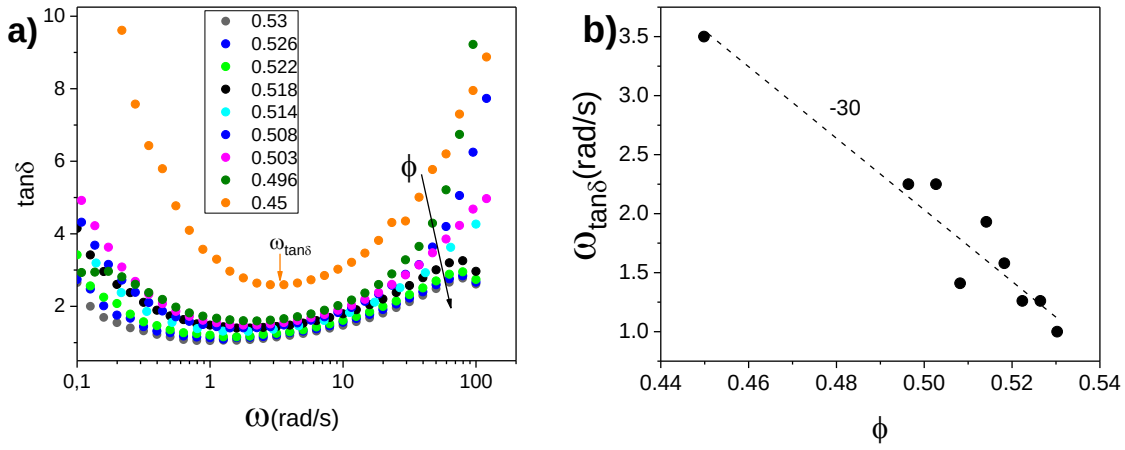

Fig. A2 LVE data for samples with $\phi < \phi_{ons} = 0.54$ where no G´, G´´ crossover is exhibited a) loss angle tangent dependence on angular frequency; different φ, as indicated, increase as shown by solid black arrow; vertical arrow indicates the minimum of tanδ (for φ=0.45) where the $\omega_{tan\delta}$ is determined. b) Frequency of the minimum in tanδ plotted as a function of ϕ. The dashed line is best data fit.

Author contributions

The authors contributed to this publication as follows: TA: Writing – original draft, Conceptualization, Investigation (experiments), Data curation. BM: Investigation (theory), Writing – review & editing, Data curation. KS: Conceptualization (theory), Writing – review & editing, Supervision (theory). GP Conceptualization, Writing – review & editing, Supervision.

View Article Online
DOI: 10.1039/D4SM01428F

Conflicts of interest

There are no conflicts to declare.

Data availability

Data for this article are available at Zenodo data repository

Acknowledgments

We thank A. B. Schofield (University of Edinburgh, UK) for kindly providing the PMMA particles. We also thank Aris Papagianopoulos (EIE, Greece) for data conversion in Fig. 1. GP and TA acknowledge support by the Twinning project FORGREENSOFT (Number: 101078989 under HORIZON WIDERA-2021-ACCESS-03). KSS acknowledges support from the Army Research Office via a MURI grant with Contract No. W911NF-21-0146.

1. Mewis J, Wagner NJ. Colloidal suspension rheology. Vol. 10. Cambridge university press Cambridge; 2012.
2. Russel WB, Russel WB, Saville DA, Schowalter WR. Colloidal dispersions. Cambridge university press; 1991.
3. Wagner NJ, Mewis J. Theory and applications of colloidal suspension rheology. Cambridge University Press; 2021.
4. Royall CP, Charbonneau P, Dijkstra M, Russo J, Smallenburg F, Speck T, et al. Colloidal hard spheres: Triumphs, challenges, and mysteries. Rev Mod Phys. 2024 Nov;96(4):045003.
5. Berthier L, Biroli G. Theoretical perspective on the glass transition and amorphous materials. Rev Mod Phys. 2011 Jun 20;83(2):587–645.
6. Berthier L, Reichman DR. Modern computational studies of the glass transition. Nat Rev Phys. 2023;1–15.
7. Biroli G, Garrahan JP. Perspective: The glass transition. J Chem Phys. 2013;138(12):12A301.

View Article Online
DOI: 10.1039/D4SM01428F

8. Li B, Lou K, Kob W, Granick S. Anatomy of cage formation in a two-dimensional glass-forming liquid. Nature. 2020;587(7833):225–9.

9. Vila-Costa A, Gonzalez-Silveira M, Rodríguez-Tinoco C, Rodríguez-López M, Rodriguez-Viejo J. Emergence of equilibrated liquid regions within the glass. Nat Phys. 2023;19(1):114–9.

10. Dauchot O, Ladieu F, Royall CP. The glass transition in molecules, colloids and grains: universality and specificity. Comptes Rendus Phys. 2024 Apr 26;24(S1):25–56.

11. Antl L, Goodwin JW, Hill RD, Ottewill RH, Owens SM, Papworth S, et al. The preparation of poly (methyl methacrylate) latices in non-aqueous media. Colloids Surf. 1986;17(1):67–78.

12. Bryant G, Williams SR, Qian L, Snook IK, Perez E, Pincet F. How hard is a colloidal "hard-sphere" interaction? Phys Rev E Stat Nonlin Soft Matter Phys. 2002 Dec;66(6 Pt 1):060501.

13. Frith WJ, Strivens TA, Mewis J. Dynamic mechanical properties of polymerically stabilized dispersions. J Colloid Interface Sci. 1990;139(1):55–62.

14. Van Megen W. Comparison of dynamic light scattering measurements and mode-coupling theory for the tagged particle dynamics of a hard-sphere suspension. Phys Rev E—Statistical Nonlinear Soft Matter Phys. 2007;76(6):061401.

15. Pusey PN. Liquids, freezing and the glass transition. North-Holland: Amsterdam; 1991.

16. Pusey PN. Colloidal glasses. J Phys Condens Matter. 2008;20(49):494202.

17. Ediger MD, Harrowell P. Perspective: Supercooled liquids and glasses. J Chem Phys. 2012;137(8):080901.

18. Donev A, Torquato S, Stillinger FH. Pair correlation function characteristics of nearly jammed disordered and ordered hard-sphere packings. Phys Rev E. 2005;71(1):011105.

19. Gotze W, Sjogren L. Relaxation processes in supercooled liquids. Rep Prog Phys. 1992;55(3):241.

20. Brady JF. The rheological behavior of concentrated colloidal dispersions. J Chem Phys. 1993;99(1):567–81.

21. Dhont JK. An introduction to dynamics of colloids. Vol. 2. Elsevier; 1996.

22. van Megan W, Underwood SM, Ottewill RH, Williams NSJ, Pusey PN. Particle diffusion in concentrated dispersions. Faraday Discuss Chem Soc. 1987;83:47–57.

23. Nägele G. Viscoelasticity and diffusional properties of colloidal model dispersions. J Phys Condens Matter. 2002;15(1):S407.

24. Johari GP. Intrinsic mobility of molecular glasses. J Chem Phys. 1973;58(4):1766–70.

View Article Online
DOI: 10.1039/D4SM01428F

25. Koumakis N, Pamvouxoglou A, Poulos AS, Petekidis G. Direct comparison of the rheology of model hard and soft particle glasses. Soft Matter. 2012;8(15):4271.

26. Mason TG, Weitz DA. Linear viscoelasticity of colloidal hard sphere suspensions near the glass transition. Phys Rev Lett. 1995;75(14):2770.

27. Mason TG, Weitz DA. Optical measurements of frequency-dependent linear viscoelastic moduli of complex fluids. Phys Rev Lett. 1995;74(7):1250.

28. Reinhardt J, Weysser F, Fuchs M. Comment on "Probing the equilibrium dynamics of colloidal hard spheres above the mode-coupling glass transition." Phys Rev Lett. 2010;105(19):199604.

29. Schweizer KS, Saltzman EJ. Entropic barriers, activated hopping, and the glass transition in colloidal suspensions. J Chem Phys. 2003;119(2):1181–96.

30. Brambilla G, El Masri D, Pierno M, Berthier L, Cipelletti L, Petekidis G, et al. Probing the equilibrium dynamics of colloidal hard spheres above the mode-coupling glass transition. Phys Rev Lett. 2009;102(8):085703.

31. Van Megen W, Mortensen TC, Williams SR, Müller J. Measurement of the self-intermediate scattering function of suspensions of hard spherical particles near the glass transition. Phys Rev E. 1998;58(5):6073.

32. Weeks ER, Weitz DA. Properties of cage rearrangements observed near the colloidal glass transition. Phys Rev Lett. 2002;89(9):095704.

33. Hallett JE, Turci F, Royall CP. Local structure in deeply supercooled liquids exhibits growing lengthscales and dynamical correlations. Nat Commun. 2018 Aug 16;9(1):3272.

34. Banchio AJ, Nägele G, Bergenholtz J. Viscoelasticity and generalized Stokes–Einstein relations of colloidal dispersions. J Chem Phys. 1999;111(18):8721–40.

35. Siebenbürger M, Fuchs M, Winter H, Ballauff M. Viscoelasticity and shear flow of concentrated, noncrystallizing colloidal suspensions: Comparison with mode-coupling theory. J Rheol. 2009;53(3):707–26.

36. Schroyen B, Vlassopoulos D, Van Puyvelde P, Vermant J. Bulk rheometry at high frequencies: A review of experimental approaches. Rheol Acta. 2020;59:1–22.

37. Hecksher T, Torchinsky DH, Klieber C, Johnson JA, Dyre JC, Nelson KA. Toward broadband mechanical spectroscopy. Proc Natl Acad Sci U A. 2017 Aug 15;114(33):8710–5.

38. Li Q, Dennis KA, Lee YF, Furst EM. Two-point microrheology and diffusing wave spectroscopy. J Rheol. 2023;67(6):1107–18.

View Article Online
DOI: 10.1039/D4SM01428F

39. Athanasiou T, Auernhammer GK, Vlassopoulos D, Petekidis G. A high-frequency piezoelectric rheometer with validation of the loss angle measuring loop: application to polymer melts and colloidal glasses. Rheol Acta. 2019;58(9):619–37.

40. Saltzman EJ, Schweizer KS. Transport coefficients in glassy colloidal fluids. J Chem Phys. 2003;119(2):1197–203.

41. Schweizer KS. Derivation of a microscopic theory of barriers and activated hopping transport in glassy liquids and suspensions. J Chem Phys. 2005;123(24).

42. Mason TG. Estimating the viscoelastic moduli of complex fluids using the generalized Stokes–Einstein equation. Rheol Acta. 2000;39(4):371–8.

43. Cipelletti L, Ramos L. Slow dynamics in glassy soft matter. J Phys Condens Matter. 2005;17(6):R253.

44. Squires TM, Mason TG. Fluid mechanics of microrheology. Annu Rev Fluid Mech. 2010;42:413–38.

45. El Masri D, Brambilla G, Pierno M, Petekidis G, Schofield AB, Berthier L, et al. Dynamic light scattering measurements in the activated regime of dense colloidal hard spheres. J Stat Mech Theory Exp. 2009;2009(07):P07015.

46. Saltzman EJ, Schweizer KS. Activated hopping and dynamical fluctuation effects in hard sphere suspensions and fluids. J Chem Phys. 2006 Jul 28;125(4):44509.

47. Luo C, Janssen LM. Glassy dynamics of sticky hard spheres beyond the mode-coupling regime. Soft Matter. 2021;17(33):7645–61.

48. Hansen JP, McDonald IR. Theory of simple liquids: with applications to soft matter. Academic press; 2013.

49. Verlet L. Integral equations for classical fluids: I. The hard sphere case. Mol Phys. 1980;41(1):183–90.

50. Verlet L. Integral equations for classical fluids: II. Hard spheres again. Mol Phys. 1981;42(6):1291–302.

51. Zhou Y, Mei B, Schweizer KS. Integral equation theory of thermodynamics, pair structure, and growing static length scale in metastable hard sphere and Weeks-Chandler-Andersen fluids. Phys Rev E. 2020;101(4):042121.

52. Chaki S, Mei B, Schweizer KS. Theoretical analysis of the structure, thermodynamics, and shear elasticity of deeply metastable hard sphere fluids. Phys Rev E. 2024 Sep;110(3):034606.

53. Hänggi P, Talkner P, Borkovec M. Reaction-rate theory: fifty years after Kramers. Rev Mod Phys. 1990;62(2):251.

View Article Online
DOI: 10.1039/D4SM01428F

54. Kramers HA. Brownian motion in a field of force and the diffusion model of chemical reactions. physica. 1940;7(4):284–304.

55. Verberg R, De Schepper IM, Cohen EGD. Viscosity of colloidal suspensions. Phys Rev E. 1997;55(3):3143.

56. Mei B, Zhou Y, Schweizer KS. Thermodynamics–structure–dynamics correlations and nonuniversal effects in the elastically collective activated hopping theory of glass-forming liquids. J Phys Chem B. 2020;124(28):6121–31.

57. Mirigian S, Schweizer KS. Elastically cooperative activated barrier hopping theory of relaxation in viscous fluids. I. General formulation and application to hard sphere fluids. J Chem Phys. 2014 May 21;140(19):194506.

58. Schweizer KS, Yatsenko G. Collisions, caging, thermodynamics, and jamming in the barrier hopping theory of glassy hard sphere fluids. J Chem Phys. 2007;127(16):164505.

59. Schaertl W, Sillescu H. Brownian dynamics of polydisperse colloidal hard spheres: Equilibrium structures and random close packings. J Stat Phys. 1994;77:1007–25.

60. Hermes M, Dijkstra M. Jamming of polydisperse hard spheres: The effect of kinetic arrest. EPL Europhys Lett. 2010 Feb 1;89(3):38005.

61. Ballesta P, Petekidis G. Creep and aging of hard-sphere glasses under constant stress. Phys Rev E. 2016 Apr;93:042613.

62. Jacob AR, Moghimi E, Petekidis G. Rheological signatures of aging in hard sphere colloidal glasses. Phys Fluids. 2019;31(8):087103.

63. Mei B, Zhou Y, Schweizer KS. Experimental test of a predicted dynamics–structure–thermodynamics connection in molecularly complex glass-forming liquids. Proc Natl Acad Sci. 2021;118(18):e2025341118.

64. Torquato S, Truskett TM, Debenedetti PG. Is random close packing of spheres well defined? Phys Rev Lett. 2000;84(10):2064.

65. Kamien RD, Liu AJ. Why is Random Close Packing Reproducible? Phys Rev Lett. 2007 Oct;99(15):155501.

66. Parisi G, Zamponi F. Mean-field theory of hard sphere glasses and jamming. Rev Mod Phys. 2010 Mar;82(1):789–845.

67. Larson RG. The structure and rheology of complex fluids. Vol. 150. Oxford university press New York; 1999.

68. Mei B, Lin TW, Sheridan GS, Evans CM, Sing CE, Schweizer KS. Structural relaxation and vitrification in dense cross-linked polymer networks: simulation, theory, and experiment. Macromolecules. 2022;55(10):4159–73.

View Article Online
DOI: 10.1039/D4SM01428F

69. Zhou Y, Mei B, Schweizer KS. Activated relaxation in supercooled monodisperse atomic and polymeric WCA fluids: Simulation and ECNLE theory. J Chem Phys. 2022;156(11).

70. Hunter GL, Weeks ER. The physics of the colloidal glass transition. Rep Prog Phys. 2012;75(6):066501.

71. Pusey PN. Colloidal Suspensions in Liquids, Freezing, and the Glass Transition: Les Houches. 1991;

72. Mei B, Zhou Y, Schweizer KS. Experimental tests of a theoretically predicted noncausal correlation between dynamics and thermodynamics in glass-forming polymer melts. Macromolecules. 2021;54(21):10086–99.

73. Ikeda A, Berthier L, Sollich P. Disentangling glass and jamming physics in the rheology of soft materials. Soft Matter. 2013;9(32):7669.

74. Mewis J, Haene P. Prediction of rheological properties in polymer colloids. In Wiley Online Library; 1993. p. 213–25.

75. Shikata T, Pearson DS. Viscoelastic behavior of concentrated spherical suspensions. J Rheol. 1994;38(3):601–16.

76. Poon WC, Weeks ER, Royall CP. On measuring colloidal volume fractions. Soft Matter. 2012;8(1):21–30.

77. Cheng Z, Zhu J, Chaikin PM, Phan SE, Russel WB. Nature of the divergence in low shear viscosity of colloidal hard-sphere dispersions. Phys Rev E. 2002;65(4):041405.

78. Sierou A, Brady JF. Accelerated Stokesian Dynamics simulations. J Fluid Mech. 2001;448.

79. Van Megen W, Underwood SM. Glass transition in colloidal hard spheres: Measurement and mode-coupling-theory analysis of the coherent intermediate scattering function. Phys Rev E. 1994;49(5):4206.

FORTH
Research • Technology • Innovation
FOUNDATION FOR RESEARCH AND TECHNOLOGY – HELLAS
INSTITUTE OF ELECTRONIC STRUCTURE AND LASER

View Article Online
DOI: 10.1039/D4SM01428F

1/12/2024

Data Availability Statement,

We would like state that Data for this article will be available at Zenodo data repository

Sincerely

For the authors
George Petekidis
Professor, Department of Materials Science and Technology, University of Crete & IESL-FORTH, Crete, Greece

Nikolaou Plastira 100
Vassilika Vouton
GR 700 13 Heraklion
Crete, Greece
Tel. +30 2810391300-2
Fax +30 2810391305
Email: iesl@iesl.forth.gr
www.iesl.forth.gr